

Integrated Ferroelectrics

An International Journal

ISSN: 1058-4587 (Print) 1607-8489 (Online) Journal homepage: <http://www.tandfonline.com/loi/ginf20>

MPB Phase Transition and Microstructure of (1 - x)PMN-xPZT Activated by 0.05BZN Ceramics

Hassakorn Wattanasarn, Wattana Photankham, Sakorn Inthachai, Tosawat Seetawan, Rattikorn Yimnirun & Chanchana Thanachayanont

To cite this article: Hassakorn Wattanasarn, Wattana Photankham, Sakorn Inthachai, Tosawat Seetawan, Rattikorn Yimnirun & Chanchana Thanachayanont (2015) MPB Phase Transition and Microstructure of (1 - x)PMN-xPZT Activated by 0.05BZN Ceramics, *Integrated Ferroelectrics*, 165:1, 19-28, DOI: [10.1080/10584587.2015.1062342](https://doi.org/10.1080/10584587.2015.1062342)

To link to this article: <http://dx.doi.org/10.1080/10584587.2015.1062342>



Published online: 22 Oct 2015.



Submit your article to this journal



Article views: 2



View related articles



View Crossmark data

Full Terms & Conditions of access and use can be found at
<http://www.tandfonline.com/action/journalInformation?journalCode=ginf20>

MPB Phase Transition and Microstructure of $(1-x)$ PMN- x PZT Activated by 0.05BNZ Ceramics

HASSAKORN WATTANASARN,¹
WATTANA PHOTANKHAM,¹ SAKORN INTHACHAI,¹
TOSAWAT SEETAWAN,^{1,*} RATTIKORN YIMNIRUN,²
AND CHANCHANA THANACHAYANONT³

¹Thermoelectrics Research Center and Program of Physics, Faculty of Science and Technology, Sakon Nakhon Rajabhat University, 680 Nittayo Rd., Sakon Nakhon 47000, Thailand

²School of Physics, Institute of Science, and COE-NANOTEC-SUT on Advanced Functional Nanomaterials, Suranaree University of Technology, Nakhon Ratchasima 30000, Thailand

³National Metal and Materials Technology Center, National Science and Technology Development Agency, 114 Thailand Science Park, Phahonyothin Rd., Klong 1, Klong Luang, Pathumthani 12120, Thailand

The relaxor ferroelectric materials can be found in morphotropic phase boundary (MPB) existing between tetragonal and cubic phase. Since the MPB shifts to other phases by adding ceramics composition. $[(1-x)\text{Pb}(\text{Mg}_{1/3}\text{Nb}_{2/3})\text{O}_3-x\text{Pb}(\text{Zr}_{0.52}\text{Ti}_{0.48})\text{O}_3]$ were doped by 0.05Ba(Zn_{1/3}Nb_{2/3})O₃ when $x = 0.4, 0.3,$ and 0.2 ceramics, which prepared by using a two-step sintering process. The MPB transitions were studied by the use of XRD. The samples, at $x = 0.4$, were in MPB and then gradually shifted to cubic phase at $x = 0.2$. The microstructure of samples fracture found that the largest grain size of $4.51\ \mu\text{m}$ for $x = 0.2$. This study using TEM technique which demonstrated a crystalline morphology with the largest crystal size about $1.293\ \mu\text{m}$ at $x = 0.3$. These results also revealed that not only the ferroelectric phase shifted to relaxor behavior with decreasing PZT contents in PMN-PZT system but also activated by BNZ, which led to the presence of the relaxor behavior.

Keywords MPB; microstructure; PMN; PZT; BNZ

1. Introduction

Mostly, Relaxor ferroelectric ceramics with lead-based complex perovskite structure are favoured by the researcher due to excellent piezoelectric properties [1, 2]. Pb(Mg_{1/3}Nb_{2/3})O₃-Pb(Zr_{0.52}Ti_{0.48})O₃ (PMN-PZT) ceramic is well known for ferroelectric materials which have been developed by researchers for portable microelectronic applications,

Received December 22, 2014; in final form May 22, 2015.

*Corresponding author; E-mail: t.seetawan@sru.ac.th

Color versions of one or more of the figures in the article can be found online at www.tandfonline.com/ginf.

such as a self-sustained battery charger and micro-electromechanical systems [3]. Recently, a member of ferroelectrics ceramic have been obtained on the basis of complex lead niobate perovskite $\text{Pb}(\text{B}_{1/3}\text{Nb}_{2/3})\text{O}_3$ (where $\text{B} = \text{Mg}^{2+}, \text{Zn}^{2+}, \text{Fe}^{3+}$). The solid state reaction process is an interesting combination of large electrostrictive responses and a minimal area hysteresis loop in the applied field [4]. Meanwhile, the regarded pyrochlore phase exists in microstructure of PMN–PZT ceramics, which decreased piezoelectric properties. The problem not only are solved by sol gel technique to suppress pyrochlore phase, but also two-step sintering with mixed oxide process [5]. However, the electrical properties and piezoelectric properties with sol gel are lower than solid state reaction. For PMN–PZT system have been focused only on $(1-x)\text{PMN}-x\text{PZT}$ when $x = 0.4, 0.3$, and 0.2 that are in morphotropic phase boundary (MPB) [6,7]. The PMN substitution into PZT has an effect to the grain size, crystal structure and electrical properties of ceramics. The PMN–PZT has been studied on phase transition dependences with PZT contents are nearly MPB composition [8]. However, in case of MPB composition, phase transition, grain shape, and crystallite shape, focus at a micro scale and nano scale of complex perovskite structure. $\text{Ba}(\text{Zn}_{1/3}\text{Nb}_{2/3})\text{O}_3$ (BZN) is one of the candidates for microwave dielectric (MD) materials that have been employed as resonators and filters for wireless communication technologies. Especially, the MD materials are able to response to the wavelength of micro and millimeter [9]. An advantage of using microwave dielectric materials is that they can be prepared with solid state reaction method, and provides the order structure in cubic perovskite. Nevertheless, low loss dielectrics and large dielectric constant are normally required at high sintering temperature sintering. Chemical processing and small particle sizes of the starting materials are needed to reduce the sintering temperature of dielectric materials [10, 11, 12]. Consequently, a coexistence of ferroelectric and microwave dielectric materials should be useful for ferroelectric materials applications.

The prepared ferroelectric material plays a crucial role for responding to the polar nano regions. In this research, the ceramics were prepared with mixed oxide composite. The PMN–PZT ceramics were obtained by columbite mixed oxide. The BZN composite were added into PMN–PZT ceramics with solid state reaction. The 0.05BZN content was selected for determining its effect on MD materials with in the PMN–PZT system. The PZT contents were also examined its effects within the PMN–PZT–BZN system. The samples were investigated in microscale such as phase transition, grain growth, crystallite characteristic, and explained the hysteresis loop and strain loop behavior that corresponded to ferroelectric properties, MPB phase transition was in the $0.95[(1-x)\text{Pb}(\text{Mg}_{1/3}\text{Nb}_{2/3})\text{O}_3-x\text{Pb}(\text{Zr}_{0.52}\text{Ti}_{0.48})\text{O}_3]-0.05\text{Ba}(\text{Zn}_{1/3}\text{Nb}_{2/3})\text{O}_3$; $0.95[(1-x)\text{PMN}-x\text{PZT}]-0.05\text{BZN}$ where $x = 0.4, 0.3$, and 0.2 .

2. Experiment

The $0.95[(1-x)\text{PMN}-x\text{PZT}]-0.05\text{BZN}$ where $x = 0.4, 0.3$, and 0.2 , were obtained by solid state reaction technique. In this study, the PMN–PZT ceramics were synthesized by columbite method. Firstly, magnesium niobate (MgNb_2O_6 ; MN) were prepared from the stoichiometric ratio for precursor, which composed of MgO (98%) with 3 mol% excess, and Nb_2O_5 (99.9%). The materials were mixed with ball milling, and fired at 1000°C for 6 h. Secondly, barium zinc niobate [$\text{Ba}(\text{Zn}_{1/3}\text{Nb}_{2/3})\text{O}_3$; BZN] obtaining ZnO (99%), Nb_2O_5 and BaCO_3 (99%) powder were mixed in ball milling for 24 h and fired 1100°C for 6 h. $(1-x)\text{PMN}-x\text{PZT}-0.05\text{BZN}$ were prepared by mixed oxide which composing of MN, PbO (99%) excess with 4 mol% for compensate PbO volatilization during heat treatment,

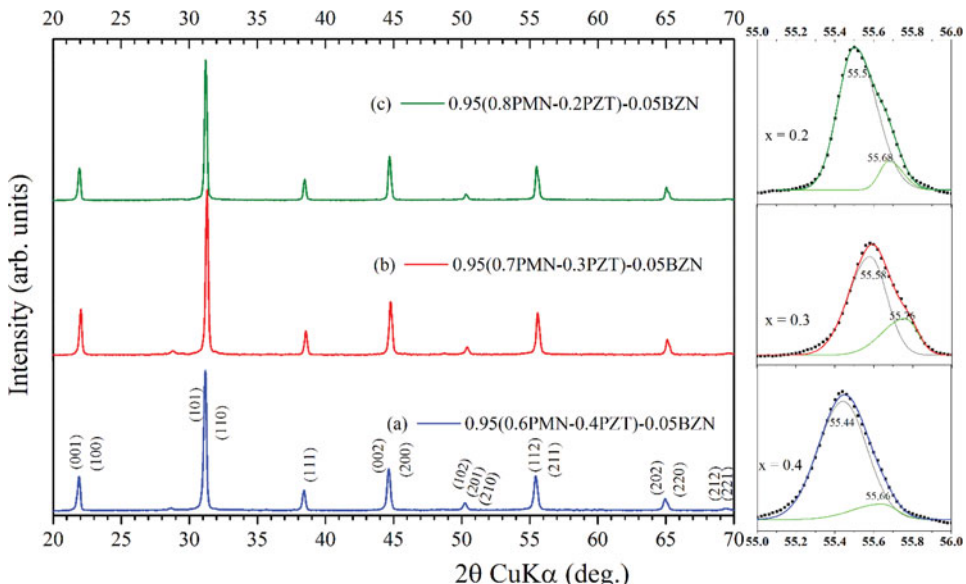


Figure 1. The illustrated of XRD patterns of $0.95[(1-x)$ PMN– x PZT]–0.05BN when $x = 0.4$, 0.3 and 0.2 ceramics, and the inset shows the transition of MPB phase to cubic phase around $2\theta = 55$ – 56° .

ZrO_2 (99%), TiO_2 (98%) and BZN. These powders were mixed again in deionize water, and then the milling process took 24 h, and vaporized by hotplate. The mixed powder was pressed through the following two-step sintering process [13]. In the first step sintering, the sample was treated in PbO atmosphere by covering the sample with PZT powder in an alumina crucible, and heated to 850°C with the heating rate of $10^\circ\text{C}/\text{min}$ and then soaked in that temperature for 4 h, and cooled at room temperature. After that the sample was crushed into powder, mixed with an aqueous solution (5%wt) of polyvinyl alcohol, and pressed into pellets at 190 MPa in form disc shape with diameter 20 mm and 1.8 mm for thickness. In the second step sintering, in order to maintain lead atmosphere during the firing process, the sample pellets were embedded in the PZT powder deriving from the previous step. The sample was sintered at 1100°C for 2 h with a heating rate of $10^\circ\text{C}/\text{min}$. After that, the sintered sample was polished to remove the lead-rich layer on the surface of sample.

The plane patterns of powder and sintered sample are determined with an X-ray diffractometer (Shimadzu XRD-6100). The XRD patterns are recorded at room temperature with $\text{Cu K}\alpha$ radiation. Diffraction intensity is measured 2θ between 20° and 70° with step up 0.02° . The density of the sample is measured by the Archimedes method. The crystal sizes are estimated by Transmission electron microscopy (TEM). The selected area electron diffraction (SAED) is performed through the use of JEOL JEM-2010, transmission electron microscope, operating at an accelerating voltage of 200 kV. Microstructure characterization is carried out on the fractured surfaces of using specimens Scanning Electron Microscopy (SEM: JEOL Model JSM-5410). A grain size of sintered sample is estimated by a linear intercept method from SEM micrographs. The surfaces of samples were coated with silver paint as an electrode for investigating hysteresis loops and strain loop, through the use of high voltage AC amplifier (Trek, model 20/20C) connecting with Sawyer-Tower circuit.

Table 1

Lattice parameters a and c , tetragonality (c/a), Rietveld refinement using data from 20 to 70° of the XRD results in Fig. 1. Crystallite sizes obtained from TEM, density, and relative theoretical density (TD)

	a (Å)	c (Å)	c/a	Crystal size (μm)	Average grain size (μm)	Density (g/cm³)	TD (%)
0.95(0.6PMN-0.4PZT)-0.05BZN	4.0255	4.0664	1.0102	0.886	2.42	7.66	94.26
0.95(0.7PMN-0.3PZT)-0.05BZN	4.0423	4.0664	1.0060	1.293	3.82	7.64	94.85
0.95(0.8PMN-0.2PZT)-0.05BZN	4.0274	4.0585	1.0077	1.113	4.51	7.592	93.33

The strain loop was estimated by micrometer displacement sensor connected with Linear Variable Differential Transformer (LVDT, Omron ZX-TDA11), the displacement signal was transmitted to a frequency filter circuit.

3. Results and Discussion

The phase structure patterns of 0.95[(1 - x)PMN-xPZT]-0.05BZN ($x = 0.4, 0.3$, and 0.2) samples were demonstrated by XRD techniques as shown in Fig. 1. The samples were identified to the characteristic patterns of complex perovskite cubic ($A(B'B'')O_3$). Usually, (1 - x)PMN-xPZT exhibits morphotropic phase boundary (MPB) for $x = 0.4$ and 0.3 , and then gradually shifting to pseudo-cubic at $x = 0.2$ [8]. In Fig. 1, the 0.05BZN content was doped into (1 - x)PMN-xPZT. The degree 2θ peak that slightly shifted to the right at $x = 0.3$, and after that shifted to the left at $x = 0.2$. This result implied that the decreasing lattice parameter was due to lattice strain as well as Zn^{2+}/Nb^{5+} ion substituting Mg^{2+}/Nb^{5+} ion in B-sites ($Pb(B_{1/3}B_{2/3})O_3$) [14], while Zr^{4+}/Ti^{4+} ion contribution decreased. Eventually, a phase transformation from the MPB phase to the pseudo-cubic phase occurs with decreasing PZT content. Using 2θ data from 20° to 70° of the XRD results, could be evaluated the lattice parameters a , c and relative density are listed in Table 1. The major differences of XRD pattern are analyzed on the peaks of (211) plane which is about 55–56°. The (211) plane is a single peak for the cubic, while (112)T and (211)T plane can be found in tetragonal phase [15]. It noted that the board peak exhibited the tetragonal phase split into two peaks at (211) plane. In order to determining the phase transition of various samples accurately, the board peak of (112) plane lines of three samples obtained by extract from XRD pattern range 55–56° are presented in Fig. 1(inset). Using Gaussian peaks (gray and green lines) fitted with the (211) reflections split to (112)T and (211)T which can be found the MPB phase for $x = 0.4$. In other words, the samples peak shifted from the left to the right of the patterns, and gradually decreased PZT content. The integrated intensity of (112)T decrease whereas the intensity of (211)T shifted to (211)C, as shown in Fig.1(inset). Apparently, the coexistence of equal quantities of the MPB region, in the tetragonal and cubic phases is

well known [16, 17]. Consequently, decreasing PZT content of 0.95(PMN–PZT)–0.05BZN was taken out of the MPB region. Although, the (211) board peaks at $x = 0.2$ is nearly equal to $x = 0.3$ with a lower intensity at $2\theta = 55.68^\circ$ of $x = 0.2$, this suggested that the MPB phase shifted to pseudo-cubic phase, besides, it was observed that the lattice ratio (a/c) decreased with decreasing PZT contents as showed in Table 1.

Figure 2 showed the mixed oxide of agglomerated nanoparticles of 0.95[(1 – x)PMN– x PZT]–0.05BZN ceramics, while the crystallite size are listed in Table 1. The crystallite shape was similar polygon for $x = 0.4$ as shown in Fig. 3(a). Meanwhile, the decreasing PZT composite in 0.95[(1 – x)PMN– x PZT]–0.05BZN. Similarly, the crystallite have been changed to a long polygon shape at $x = 0.3$ which was illustrated in Fig. 3(b). The larger size of when $x = 0.2$ was illustrated in Fig. 3(c). In addition, stacking faults, occurred from the polycrystalline of complex perovskite structure were used to observe the samples (white arrow) as shown in Fig. 3(a–c). This suggested that the increased atomic species affected the crystalline structure in term of difficulty for arranging the constituent atoms into ordered structure [18]. The formation processes of nanoscale oxide particles of 0.95[(1 – x)PMN– x PZT]–0.05BZN formed the amorphous structure as follows respectively: crystalline structure, disordered structure due to loss of long-range order, fine grained in nanocrystalline structure, and amorphous structure of complex perovskite [19,20].

The SAED diffraction patterns of polycrystalline materials involved the interplanar distances obtaining patterns of 0.95[(1 – x)PMN– x PZT]–0.05BZN ceramics which were illustrated in Fig. 2 (insets), the decreased PZT contents affecting the diffraction rings. Instead, the well-defined (bright spots are typical from radius of the rings) corresponded to the d-spacings of 0.95[(1 – x)PMN– x PZT]–0.05BZN ceramics. The results matched well with that of XRD pattern. The SAED of $x = 0.4$ (inset in Fig. 2(a)) exhibited a circular rings which was drawn passing the small bright spots dispersing around a big bright spot. This result indicated that coexistence of tetragonal phase and cubic phase. Furthermore, the ring diffraction patterns exhibited a polycrystalline ceramic. Consequently, the total energy is conserved in the diffracted and direct transmitted beams that extracted from the sample [21]. The dispersion of small bright spots decreased with decreasing PZT contents for $x = 0.3$ (see inset in Fig. 2 (b)). This result suggested that PMN–PZT–BZN system reduced the proportion of MPB phase and transformed to cubic phase. In Fig. 2 (c) (inset), the dispersion of small bright spots and decreased when $x = 0.2$. The investigated plane patterns and the circular rings were drawn passing the bright spots which can be clearly seen. It notes that long-range order of PZT affects to PMN–PZT–BZN exhibits cubic perovskite phase. This result corresponds to XRD patterns and nano particle behavior.

The fractured surface micrographs of 0.95[(1 – x)PMN– x PZT]–0.05BZN ($x = 0.4$, 0.3, and 0.2) ceramics were determined by using SEM technique as shown in Fig. 3. The morphology of the 0.95[0.6PMN–0.4PZT]–0.05BZN fracture surface is illustrated in Fig. 3(a). Generally, PZT powder consists of agglomerates with larger polygon grain [9]. The 0.6PMN–0.4PZT consists of very fine grains, and loose agglomerates, However, 0.95[0.6PMN–0.4PZT]–0.05 BZN ceramic exhibited a grain feature similar to polygon shape, it notices that some of PZT could not agglomerates with BZN as well as may be respond to the ferroelectric properties. Fig 3(b) show SEM micrographs of 0.95[0.7PMN–0.3PZT]–0.05BZN ceramic, The result revealed that the PMN and BZN composites changed a grain shape from fine grain to larger grain due to agglomerated of Mg^{2+}/Nb^{5+} ions with Zn^{2+}/Nb^{5+} ions, whereas some polygon grains of PZT disappear at $x = 0.3$. Finally, Fig 3(c) further addition PZT for $x = 0.2$ into the composition leading to

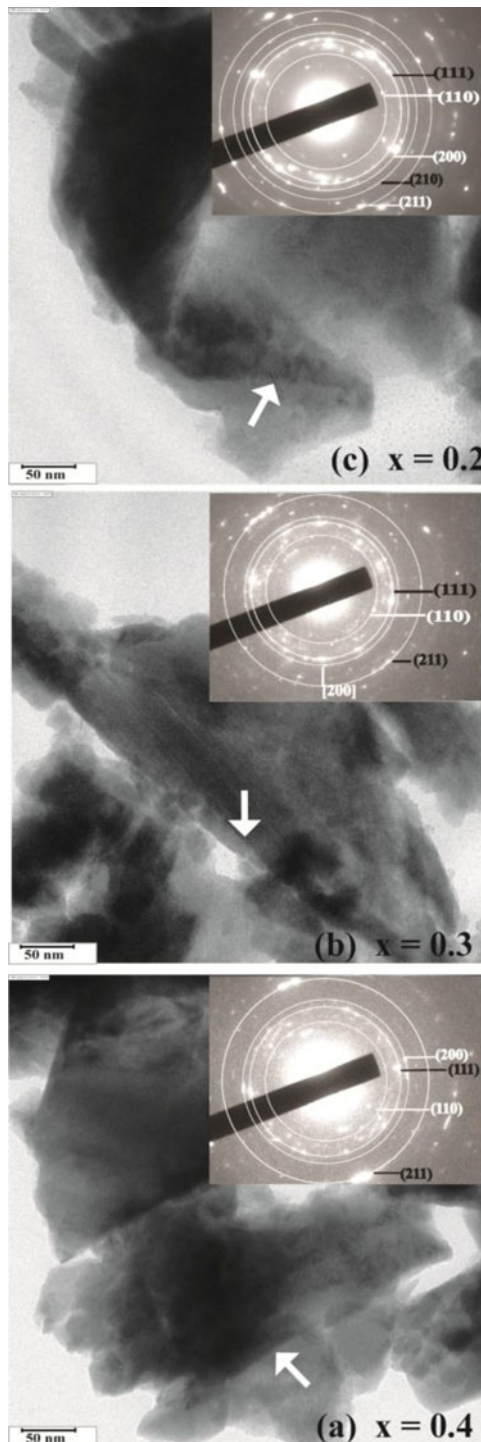


Figure 2. The morphology of $0.95[(1-x)\text{PMN}-x\text{PZT}]-0.05\text{BZN}$ ceramics by TEM technique with the corresponding selected area electron diffraction (SAED) patterns (insets) and stacking faults (with the arrow), (a) 0.4, (b) 0.3, and (c) 0.2.

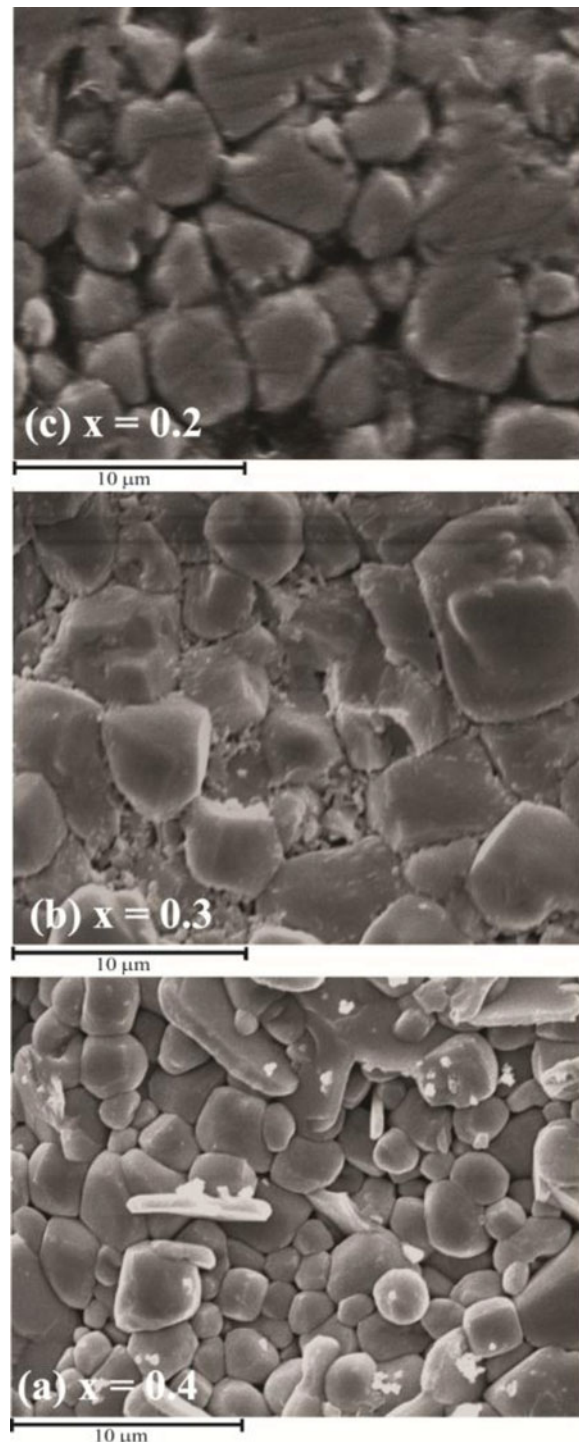


Figure 3. SEM micrographs from fractured surface of $0.95[(1 - x)\text{PMN} - x\text{PZT}] - 0.05\text{BZN}$ ceramics sintered at 1100°C while x is equal to (a) 0.4, (b) 0.3, and (c) 0.2.

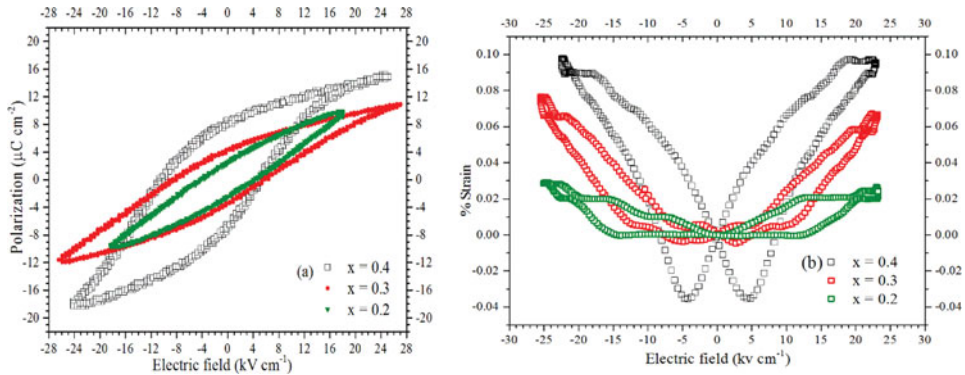


Figure 4. Illustrating the applied electric field into $0.95[(1-x)\text{PMN}-x\text{PZT}]-0.05\text{BZN}$ ceramics (a) polarization at 100 Hz tested electric field at 25 kV/cm and (b) electromechanical strain at 10 Hz for various compositions tested at 20 kV/cm .

decreasing grain size. This is may be result from the sintering temperature, and decreasing PZT content in $0.95[(1-x)\text{PMN}-x\text{PZT}]-0.05\text{BZN}$ system [15].

Table 1 exhibited the percentages of relative densities and experiment densities of sintering of $0.95[(1-x)\text{PMN}-x\text{PZT}]-0.05\text{BZN}$ ($x = 0.4, 0.3,$ and 0.2) ceramics. It noted that the relative densities slightly increases with decreasing PZT content of $0.95[(1-x)\text{PMN}-x\text{PZT}]-0.05\text{BZN}$ from $x = 0.4$ to $x = 0.3$. The lowest relative densities for $x = 0.2$ since increasing of porous was illustrated in Fig. 3(c). This suggested that either the addition of a larger particle size of 0.05BZN into the $(1-x)\text{PMN}-x\text{PZT}$ composition or temperature sintering which decreases significantly the density of the bulks [9 10]. As shown in Table 1, the lowest of grain size was found at $x = 0.4$. The grain size varied from 2.42 to $4.51 \mu\text{m}$. Although, the reason for the changing of the density and grain sizes could not be clearly indicated in the mixed oxides, the results exhibit that temperature sintering is a inhibition of grain-growth in solid state reaction process [8, 10].

The polarization hysteresis loop for the $0.95[(1-x)\text{PMN}-x\text{PZT}]-0.05\text{BZN}$ composition exhibited a characteristic that approaching the soft relaxor ferroelectric behavior (Fig. 3), including the phase transitions from ferroelectric phase to anti-ferroelectric phase. A polarization hysteresis loop ($P - E$) and strain loop ($S - E$) are indicated to domain switching, and a typical of relaxor ferroelectric with decreasing PZT content. The polarization loops exhibited a slim loop at $x = 0.4$, remnant polarization (P_r) and saturated polarization (P_s) decreased with decreasing PZT content as shown in Fig. 4(a). The strain loops for the $0.95[(1-x)\text{PMN}-x\text{PZT}]-0.05\text{BZN}$ composition showed a typical pinched loop, which was a characteristic of relaxor ferroelectric behavior as illustrated in Fig. 4(b). Usually, domain in polar nano regions (PNRs) induces irreversibly on applied electric field [22]. However, there were two possible explanations which were consistent with the smaller area of polarization loop and pinching of the strain loop as $x = 0.2$. Firstly, $P - E$ and $S - E$ did not switched the domain in PNRs for these compositions. Secondly, the compositional samples were disordered because of a long-range order within the inhomogeneous of nano regions [23]. In addition, the strain increased with increasing PZT content. The effective piezoelectric coefficient (d_{33}^*), which was determined from slope of strain loop, showed the highest of $P_r = 8.21 \mu\text{C/cm}^2$ and $d_{33}^* = 16.83 \text{ pm/V}$ at $x = 0.4$. The results showed that

piezoelectric coefficient of PMN-PZT-BZN decreased for relaxor ferroelectric properties, due to cubic phase of BZN agglomerated with MPB phase of PMN-PT and caused the decrease of ferroelectric properties.

4. Conclusions

Modifying PZT in $0.95[(1 - x)\text{PMN}-x\text{PZT}]-0.05\text{BN}$ ($x = 0.4, 0.3,$ and 0.2) ceramics were prepared by the two-step sintering process. The phase transitions have been studied using X-ray diffraction technique. When decreasing PZT contents, the structures of the PMN-PZT-BZN structure experienced a gradual transition process from MPB phase to cubic phase. Crystallite sizes of the samples were in a range $0.886\text{--}1.293\ \mu\text{m}$ through the use of TEM technique. The largest grain size at $4.51\ \mu\text{m}$ for $0.95[0.8\text{PMN}-0.2\text{PZT}]-0.05\text{BN}$ was obtained, and then decreased with decreasing PZT contents. Domain switching in nano regions, observed through the saturated polarization, remnant polarization and coercive field values decreases with decreasing PZT, such a slight transition of ferroelectric phase to relaxor ferroelectric phase. The strain loop showed that decreasing PZT contents leading to relaxor phase. These results confirmed the preparation of a bulk ceramics, which affects micro-scaled and nano-scaled transitions with gradual PZT contents. These results also attribute to ferroelectric and relaxor ferroelectric behavior, and will be useful for actuator and capacitor applications.

References

1. L. E. Cross, Ferroelectric materials for electromechanical transducer applications, *Mater. Chem. Phys.* **43**, 108–115 (1996).
2. K. Vladimír, A. Carlos, B. Jaroslav, B. Helena and S. Karol, Effect of PMN modification on structure and electrical response of $x\text{PMN}-(1-x)\text{PZT}$ ceramic systems, *J. Eur. Ceram. Soc.* **23**, 1157–1166 (2003).
3. H. S. Kim, J. H. Kim and J. Kim, A Review of Piezoelectric Energy Harvesting Based on Vibration, *Inter. J. Preci. Engineer. Manu.* **12** (6), 1129–1141 (2011).
4. V. Koval, C. Alemany, J. Briancin, H. Brunckova and K. Saksl, Effect of PMN modification on structure and electrical response of $x\text{PMN}-(1-x)\text{PZT}$ ceramic systems, *J. Eur. Ceram. Soc.* **23**, 1157–1166 (2003).
5. P. Moetakef and Z. A. Nematib, Study of microstructure and dielectric properties of PMN-PZT ceramics via a mixed powder method including sol–gel precursor, *J. Alloy Compd.* **476**, 791–796 (2009).
6. M. Sebastian, *Dielectric Materials for Wireless Communication, 1st Edition*, Elsevier, (2008).
7. S. F. Wang, Y. R. Wang, C. Y. Liu and W. S. Hsieh, Microwave dielectric properties of multi-ions $\text{Ba}(\text{Zn},\text{Ta})\text{O}_3$ based perovskite ceramics, *Ceram. Int.* **38** 1127–1132 (2012).
8. R. Yimnirun, S. Ananta and P. Laoratanakul, Dielectric and ferroelectric properties of lead magnesium niobate–lead zirconate titanate ceramics prepared by mixed–oxide method, *J. Eur. Ceram. Soc.* **25**, 3235–3242 (2005).
9. H. Hughes, D. M. Iddles and I. M. Reaney, Niobate–based microwave dielectrics suitable for third generation mobile phone base stations, *Appl. Phys. Lett.* **79**, 2952–2954 (2001).
10. T. Kakada, S. F. Wang, Syoshikawa, S. T Jang and R. E. Newnham, Effect of glass . . . microwave ceramics, *J. Am. Ceram. Soc.* **77**, 1909 (1994).
11. S. I. Hirno, Takashi, Hayashi and A. Hattori, Chemical Processing and Microwave Characteristics of $(\text{Zr},\text{Sn})\text{TiO}_4$ Microwave Dielectrics, *J. Am. Ceram. Soc.* **74**, 1320 (1991).
12. V. Tolmer and G. Desqardin, Low-temperature sintering and influence of the process . . . properties of $\text{Ba}(\text{Zn}_{2/3}\text{Ta}_{2/3})\text{O}_3$, *J. Am. Ceram. Soc.* **80**, 1981 (1997).

13. P. Moetakef and Z. A. Nemat, Synthesis of PMN pyrochlore free ceramics via a modified mixed oxide method, *J. Electroceram.* **19**, 207–213 (2007).
14. L. L. Hsiung, M. J. Fluss, S. J. Tumey, B. W. Choi, Y. Serruys, F. Willaime and A. Kimura, Formation mechanism and the role of nanoparticles in Fe–Cr ODS steels developed for radiation tolerance, *Phys. Rev. B.* **82**, 184103 (2010).
15. D. G. Morris and M. A. Morris, Microstructure and strength of nanocrystalline copper alloy, *Acta Meta. Mater.* **39**, 1763–1770 (1991).
16. C. Suryanarayana, E. Ivanov and V. V. Boldyrev, The science and technology of mechanical alloying, *Mater. Sci. Eng. A.* **304-306**, 151–158 (2001).
17. D. Brandon and W. D. Kaplan, *Microstructural Characterization of Materials 2nd Edition*, Technion, Israel Institute of Technology, Israel, John Wiley & Sons Ltd. pp. 224 (2008).
18. J. P. Guha, Reaction Chemistry and Subsolidus Phase Equilibria in Lead Based Relaxor Systems, *J. Mater. Sci.* **34**, 4985–4994 (1999).
19. D. G. Morris and M. A. Morris, Microstructure and strength of nanocrystalline copper alloy, *Acta Meta. Mater.* **39**, 1763–1770 (1991).
20. C. E. Ciomega, A. M. Neagu, M. V. Pop, M. Airimioaei, S. Tascu, G. Schileo, C. Galassi and L. Mitoseriu, Ferroelectric and dielectric properties of ferrite–ferroelectric ceramic composites. *J. Appl. Phys.* **113**, 074103 (2013).
21. D. K. Dass Gupta and P. C. N. Scarpa, Modeling of dielectric relaxation spectra of polymers in the condensed phase. *Elec. Ins. Mag.* 1523–32 (1999).
22. H. Dong, X. J. Zheng, W. Li, Y. Q. Gong, J. F. Peng and Z. Zhu, The dielectric relaxation behavior of $(\text{Na}_{0.82}\text{K}_{0.18})_{0.5}\text{Bi}_{0.5}\text{TiO}_3$ ferroelectric thin film. *J. Appl. Phys.* **110**, 124109 (2011).
23. H. N. Tailora, A. A. Bokova and Z. -G. Yea, Synthesis and Dielectric Characterization of a New Relaxor Solid Solution of $(1-x)\text{Pb}(\text{Mg}_{1/3}\text{Nb}_{2/3})\text{O}_3-x\text{Bi}(\text{Zn}_{1/2}\text{Ti}_{1/2})\text{O}_3$. *Ferroelectrics.* **405**, 67–75 (2010).